ELSEVIER

Journal of Nuclear Materials 266–269 (1999) 380–385

journal of nuclear materials

Enhanced confinement discharges in DIII-D with neon and argon induced radiation

G.L. Jackson [a,*], M. Murakami [b], G.M. Staebler [a], M.R. Wade [b], A.M. Messiaen [c], J. Ongena [c], B. Unterberg [d], J.A. Boedo [e], T.E. Evans [a], A.W. Hyatt [a], R.J. LaHaye [a], C.J. Lasnier [f], A.W. Leonard [a], G.W. McKee [g], R. Maingi [b], R.A. Moyer [e], T.W. Petrie [a], W.P. West [a]

[a] *General Atomics, P.O. Box 85608, San Diego, CA 92186-9784, USA*
[b] *Oak Ridge National Laboratory, Oak Ridge, TN, USA*
[c] *ERM, Brussels, Belgium*
[d] *Forschungszentrum, Jülich, Germany*
[e] *University of California, San Diego, USA*
[f] *Lawrence Livermore National Laboratory, Livermore, CA, USA*
[g] *University of Wisconsin, Madison, WI, USA*

Abstract

Enhanced energy confinement in discharges with impurity induced radiating power fractions, P_{rad}/P_{in}, from 50% to 100% have been observed in the DIII-D tokamak with neon and argon gas puffing. These radiating mantle enhanced confinement discharges have been obtained in the DIII-D tokamak under a variety of conditions: diverted and limited configurations with both an H-mode and L-mode edge. Confinement enhancements as high as the ELM free H-mode scaling relation have been obtained with impurity gas puffing, although operation at the highest densities is transient. Similarities and differences between these DIII-D discharges and RI-mode discharges obtained in the TEXTOR tokamak are discussed.

Keywords: DIII-D; Tokamak operations; Neon; Graphite

1. Introduction

Reactor operating scenarios where a substantial fraction of the plasma energy is radiated in a mantle around the core of the plasma can be important in reducing the heat flux to plasma facing surfaces and hence controlling the erosion of these surfaces. If high density and high confinement operation accompany the radiating mantle then this solution is especially attractive for fusion ignition devices such as ITER if the nonintrinsic impurities can be minimized in the plasma core. Experiments in the DIII-D tokamak have demonstrated that radiating mantle discharges with these characteristics can be achieved, albeit on a transient basis. In the work reported here we have obtained discharges with a radiating fraction, $P_{rad,tot}/P_{in} \leqslant 1$, and normalized densities, n_e/n_{GW} up to 0.74 (limiter L-mode) and 0.95 (diverted H-mode).

Previously, discharges with non-intrinsic impurity radiation have been used in various experimental devices to demonstrate improved confinement above L-mode with increased radiation: Z-mode in ISX-B [1], RI-mode in TEXTOR [2], CDH-mode in ASDEX-U [3], IH-mode in JFT-2M [4]. In the present work we extend radiating mantle scenarios to a larger machine, DIII-D. The DIII-D radiating mantle discharges discussed here were obtained in both inside wall limited and divertor discharges. Limiter discharges are discussed in Section 2

* Corresponding author. Tel.: +1-619 455 2157; fax: +1-619 455 4156; e-mail: jackson@gav.gat.com.

0022-3115/99/$ – see front matter
PII: S0022-3115(98)00653-9

and diverted discharges in Section 3. Comparison to RI-mode work in TEXTOR and further discussion is presented in Section 4.

2. Limiter radiating mantle discharges in DIII-D

The DIII-D tokamak can produce both inside wall limited and divertor configurations. A typical L-mode inner wall limited (IWL) discharge with impurity puffing is shown in Fig. 1. Limited discharges in DIII-D contact the inner wall and are unpumped since the toroidally continuous cryopumps are located in the ceiling and floor and are designed to pump the outer leg of diverted discharges. The discharge evolution shown in Fig. 1 exhibits many phases, described below, leading up to the radiating mantle phase. After current flattop (1400 ms), argon injection (Fig. 1(b)) was started at $t = 1500$ ms during the L-mode phase of the discharge. H-mode transitions began at 1680 ms, with the H-mode confinement enhancement, $H = \tau_E/\tau_{ITER89P}$ shown in Fig. 1(d), limited by frequent L-mode phases. The

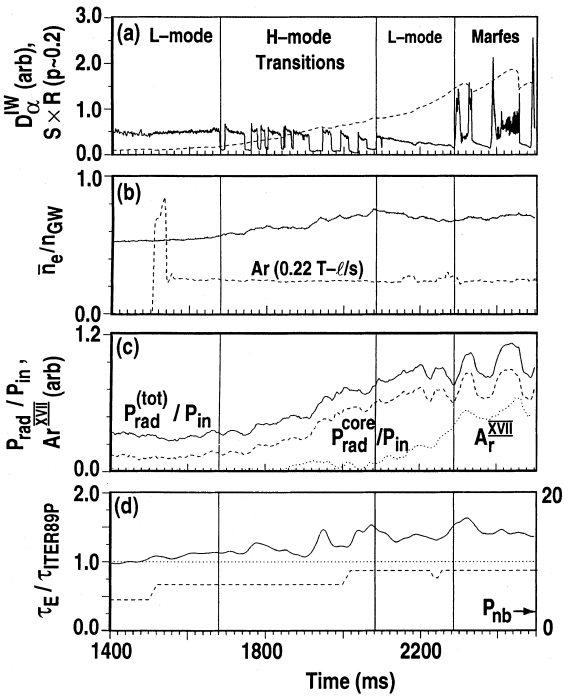

Fig. 1. Time evolution leading to the radiating mantle phase of a IWL discharge in DIII-D: (a) Inner wall D_α intensity and central soft X-ray emission; (b) normalized density, n_e/n_{GW} and argon impurity flow (there was no deuterium puffing during the time shown); (c) radiation fractions and ArXVII line intensity which was the dominant charge state, and (d) H-factor and neutral beam power. Discharge conditions (#95758): 1.3 MA, 1.8 T, $\kappa \approx 1.5$.

steady argon flow caused a slow increase in radiated power until 1920 ms when there was a marked increase in both the total radiated power and mantle radiation (Fig. 1(c)). After increasing the neutral beam heating power to 8.7 MW at 2000 ms an L-mode phase ensued and the H-factor varied between $1.3 < H < 1.5$. Density remained nearly constant during this L-mode phase (Fig. 1(b)) with $n_e/n_{GW} > 0.65$. Since there was a continuous argon flow in this unpumped discharge, radiated power continued to increase until MARFing began at 2290 ms. This phase is characterized by a marked increase in the inner wall D_α line intensity shown in Fig. 1(a). In this discharge, the MARFes caused no degradation in either confinement or density although we note that MARFing can reduce confinement under some conditions, e.g. a high D_2 gas puffing rate to increase density. During the period when MARFing was observed, the heat pulse from sawtooth crashes (Fig. 1(a)) momentarily stopped the MARFing. The temporal behavior of an ArXVII charge exchange impurity line, the main contributor to Z_{eff}, is plotted in Fig. 1(c). In this discharge core Z_{eff} varied from 1.4 to 2.3 during the L-mode phase, but increased to as high as 3.8 during the MARFing phase, although there was no degradation in confinement (Fig. 1(d)). Core Z_{eff} is calculated from the charge exchange recombination line emission of the dominant impurities, C^{+6}, Ar^{+18}, Ar^{+17}, and Ar^{+16} measured by the SPRED UV spectrometer.

Fig. 2 compares two discharges with and without impurity puffing. External programming for these discharges was identical except for the argon injection. Both discharges had an early L-mode phase (not shown) followed by H-mode. The discharge without impurities remained in "dithering" H-mode (Fig. 2(b)) while the radiating mantle discharge (the same as Fig. 1) exhibited periods of L-mode behavior. Note that during the L-mode (including MARFing) phase ℓ_i increased, up to 1.35. Density remained as high or higher than the reference (non radiating) ELMing H-mode discharge. In typical DIII-D discharges without impurity radiation, a transition from H-mode to L-mode produces a marked decrease in density since particle confinement time is substantially reduced while external particle sources are unchanged. Stored energy and confinement in the radiating mantle discharge are slightly higher than the reference H-mode discharge. Another feature of these radiating mantle discharges is an increase in toroidal rotation during the L-mode phase, shown in Fig. 2(d).

The radiating improved confinement mode (RI-mode) in limiter discharges has been extensively studied on the TEXTOR tokamak [2]. Fig. 3 plots the TEXTOR RI-mode scaling relation and compares this to DIII-D IWL discharges with either neon or argon impurity seeding. At present the DIII-D database is not large enough to observe confinement scaling, but the confinement is generally higher than TEXTOR discharges

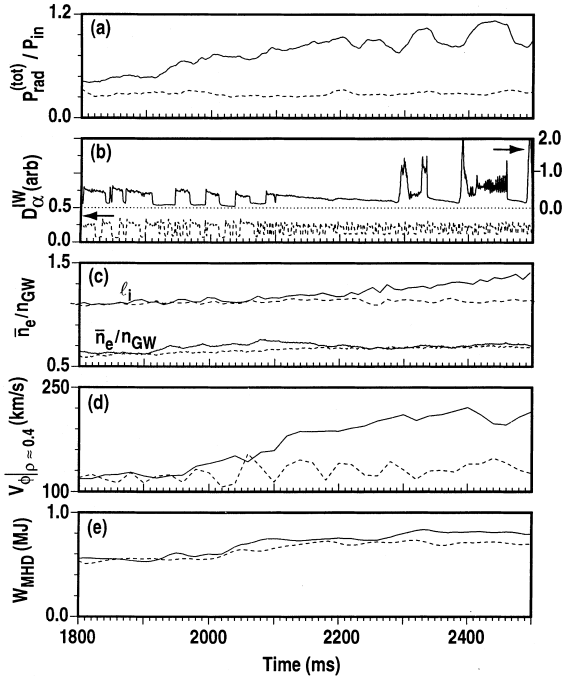

Fig. 2. Comparison of a discharge with impurity injection (#95758, solid) to a similar discharge with no impurity puff (#95756, dashed). Stored energy, W_{MHD}, and ℓ_i are calculated from EFIT equilibria including motional Stark effect measurements and toroidal rotation is measured by charge exchange recombination of a visible CVI line.

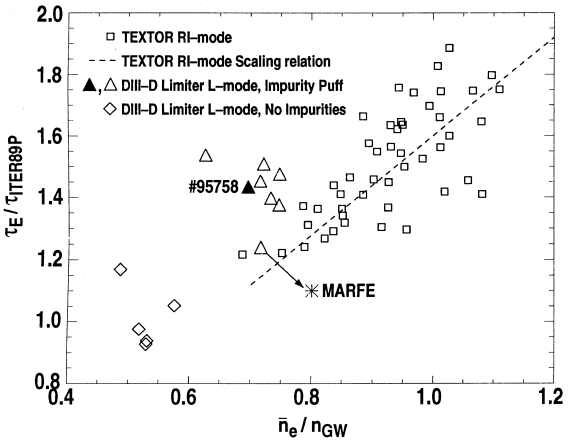

Fig. 3. A comparison of the energy confinement enhancement, H, as a function of normalized density for both DIII-D and TEXTOR discharges. The confinement degradation of one discharge (#95742) after MARFing began is shown by an arrow.

at the same normalized density. This will be discussed more in Section 4. The DIII-D radiating mantle limiter discharges obtained to date were at normalized densities at the lower range for TEXTOR RI-mode. Increasing the deuterium gas puffing rate to obtain higher densities often led to MARFing and degraded confinement. An example of such behavior is shown in Fig. 3 (arrow) where a discharge evolved from L-mode to a MARFing phase.

3. Divertor radiating mantle discharges in DIII-D

An example of a diverted radiating mantle discharge compared to a discharge with radiation primarily in the divertor region is shown in Fig. 4. All external conditions were the same for these 2 discharges, i.e. lower single-null divertor (LSN) with pumping, $I_p = 1.3$ MA, $B_t = 2.1$ T, $S_{deuterium} = 150$ T l/s and $S_{argon} = 0.9$ T l/s. Both of these discharges were pumped by the lower DIII-D liquid helium cryo pump. Neutral beam power was feedback controlled to maintain constant stored energy and varied slightly in these 2 shots. At about 2.8 s there is a marked increase in radiation in one of these discharges (#95011). After this transition, toroidal plasma rotation increases and density continues to in-

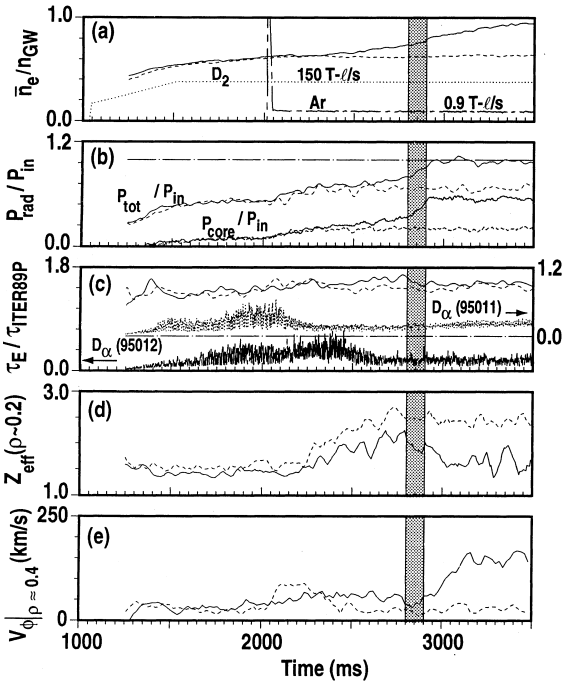

Fig. 4. Comparison of two similar discharges, one which transitions into a radiating mantle (#95011, solid) and one which has primarily divertor radiation (#95012, dash). The transition region is shown by the shaded area. The calculation of core Z_{eff} is discussed in Section 2. Deuterium and argon gas puffing rates are the same for both discharges. Discharge conditions are: 1.3 MA, 2.1 T, lower single-null divertor with pumping.

crease to nearly the Greenwald limit (Fig. 4(a)) while the confinement enhancement shows no decrease below the comparison discharge (#95012). Both discharges were ELMing H-mode throughout the times shown in Fig. 4. Central Z_{eff} is less than 2 for the radiating mantle discharge. Internal inductance, ℓ_i, is ~5% higher for the radiating mantle discharge (#95011) after the transition when compared to #95012.

Some edge characteristics of these discharges are presented in Fig. 5. Coincident with the transition to higher mantle radiation, electron temperature near the LCFS decreases (Fig. 5(a)) and the ion saturation current at the outer strike point is reduced (Fig. 5(c)) when compared with the radiating divertor case (Fig. 5(d)). Peak heat flux conducted to the divertor plates, measured by the Infrared TV cameras also decreases nearly a factor of two after the radiating mantle transition (Fig. 5(e)).

Electron temperature and density measured by Thomson scattering and ion temperature and impurity profiles calculated from charge exchange recombination spectroscopy (CER) are shown in Fig. 6. After the transition to a radiating mantle, the density profile becomes more peaked. As shown in Fig. 6, $T_e \approx T_i$, as would be expected from the short ion–electron equilibration times at these high densities. The C^{+6} impurity fraction is shown in Fig. 6(c). Argon impurity fractions (not shown) are hollow, but a quantitative calculation of the argon density, which exists in multiple charge states, requires modeling and has not been completed.

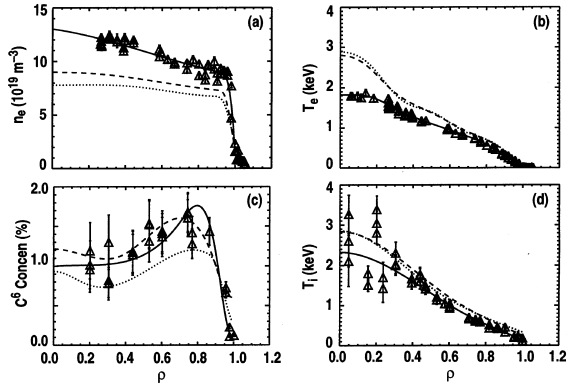

Fig. 6. Profiles during the evolution of the radiating mantle discharge (#95011) at 3 times: 1960 ms before argon injection (dots), 2700 ms just before the transition (dashed), and 3400 ms with a strongly radiating mantle (solid). For clarity, data points are only shown for the fits at 3400 ms. Electron density (a) is measured by Thomson scattering and T_e (b) is determined from fits to Thomson scattering and 3rd harmonic ECE measurements. The C^{+6} impurity fraction (c) and T_i (d) are calculated from CER measurements.

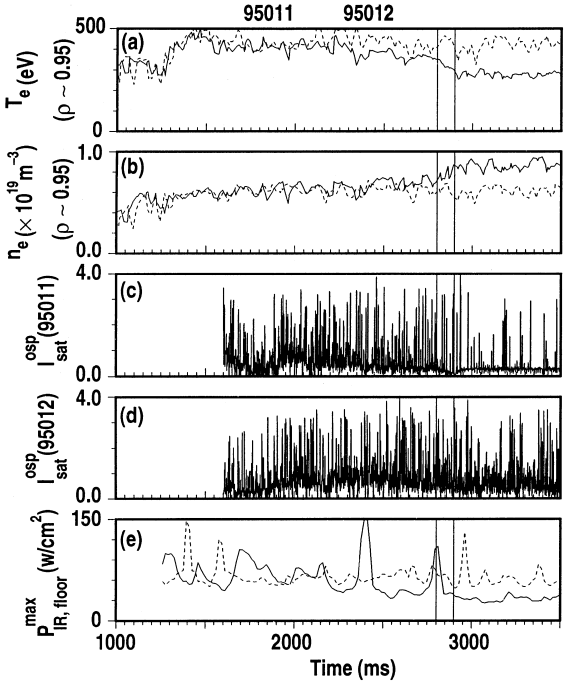

Fig. 5. A comparison of mantle and divertor parameters for the radiating mantle (#95011, solid) and a discharge with divertor radiation (#95012, dash): (a) T_e approximately 3 cm inside the LCFS; (b) n_e at the same position, both measured by Thomson scattering. The ion saturation current from a Langmuir probe near the outer strike point (at the pump aperture) is shown in (c) for #95011 and (d) for #95012. Peak heat flux in the lower divertor is displayed in (e).

4. Discussion

The limiter L-mode radiating mantle discharges obtained in DIII-D have some of the characteristics observed in the TEXTOR radiating improved confinement mode (RI-mode). This is summarized in Table 1, using DIII-D discharge #95758, displayed as a solid triangle in Fig. 3, for comparison. However, as illustrated by the example in Table 1, we have not yet achieved "stationary" discharges at the highest values of radiated power ($P_{\text{rad}}/P_{\text{in}} > 0.8$) and density ($n_e/n_{\text{GW}} > 0.9$), where TEXTOR reports the highest confinement [2]. We note that stationary discharges (not presented in this paper) have been achieved at the lower end of the parameter range shown for TEXTOR in Table 1, but without high density stationary discharges in DIII-D, we cannot evaluate the TEXTOR RI-mode scaling relation, namely $\tau_E/\tau_{H93} \propto n_e/n_{\text{GW}}$, where τ_{H93} is the ITER 93H ELM free scaling relation. However, at the same normalized density, shown in Fig. 3, normalized confinement is generally higher in DIII-D than TEXTOR. Although κ is

Table 1
Comparison of TEXTOR and DIII-D RI-mode discharges

	TEXTOR RI-mode (1992–1998)	DIII-D #95758 (2.1–2.5 s)
P_{rad}/P_{in}	0.50–1	0.8–1.0
n_e/n_{GW}	0.7–1.2	0.65–0.75
τ_E/τ_{H93}	0.8–1.2	0.9–1.0
$P_{nb}(CO)/P_{in}$	>0.25	1.0
q_{95}	2.5–5	3.5–3.8
RI-mode duration, $\Delta t/\tau_E$	>100	4.7
Non-intrinsic impurities	Ne,Ar,Si	Ar

higher in the DIII-D experiments, this is accounted for in the ITER89P scaling relation and cannot explain this difference. Although DIII-D discharges are not stationary, phases lasting several energy confinement times have been obtained, e.g. Table 1, and no apparent degradation has been observed. Hence reason for the difference in normalized confinement between TEXTOR and DIII-D is not known and is currently being investigated.

High density operation in DIII-D IWL L-mode discharges is limited by MARFEs induced by high deuterium gas puffing rates, which has also been observed in TEXTOR [5]. In addition TEXTOR reports that horizontal position of the plasma is important in achieving their high density RI-modes, which limit on the outer ALT II pumped limiter [6]. For DIII-D, operational improvements are being considered to allow operation on the outboard limiters with the goal of extending radiating mantle limiter regimes to higher density and steady state operation.

DIII-D *diverted* discharges with a radiating mantle also show the promise of being an attractive scenario for ITER. In these discharges density approached the Greenwald limit but confinement did not degrade and central Z_{eff} generally remained less than 2.5. We note, however that these discharges have not achieved steady state. For the discharge in Fig. 4, the radiative fraction reached 100% and a radiative collapse occurred ($t > 3.5$ s) accompanied by a large influx of impurities. To date, no feedback has been used to control the radiated power fraction, although it is planned for future experiments. Radiating mantle diverted discharges had a significantly reduced peak heat flux to the divertor plates, e.g. Fig. 5, and even though this was an ELMing H-mode discharge, ELMing activity measured by the ion saturation current from a Langmuir probe at the outer strike point was significantly reduced during the radiating mantle phase. While heat and particle fluxes are reduced, these radiating mantle discharges are not completely detached.

Many of the discharges with mantle radiation show an increase in toroidal plasma rotation, similar to those displayed in Figs. 2 and 4. The largest increase in rotation occurs well inside the LCFS ($\rho \approx 0.4$) and in many cases coincides with an increase in density. The increase in rotation and the rotational shear during the radiating mantle phase is characteristic of the spin-up first observed in DIII-D in very high confinement VH-mode discharges [7], although the magnitude of this rotation is less than in VH-mode discharges. We note that VH-mode is ELM free, while the radiating mantle discharges discussed here are either L-mode or have an ELMing H-mode edge. Further experiments are needed to elucidate the role of rotation in DIII-D radiating mantle discharges.

Another characteristic of many puff and pump radiating mantle discharges is a decrease in Z_{eff} after the transition, e.g. Fig. 4. Part of this decrease may be the higher density, but the temporal behavior of core Z_{eff} and n_e is not the same. We are examining the possible role of an outward neoclassical pinch in reducing the core Z_{eff}.

A concern for reactor scenarios with non-intrinsic impurity injection is that core impurities will reduce the hydrogenic fraction and limit neutron reactivity. While this was sometimes a problem in the present work, there are many examples where the core Z_{eff} was less than 2, e.g. Fig. 4. Even the limiter L-mode discharge shown in Figs. 1 and 2, Z_{eff} was less than 2.3 before MARFing began. We note that sawteeth may limit core impurity accumulation. For example core argon was substantially reduced after the sawtooth crashes in Fig. 1, although energy confinement was not degraded.

Although we have described one diverted and one limited radiating mantle discharge with argon in detail, comparable behavior has been observed with either neon or argon puffing. Radiating mantle discharges with $H > 1.5$ have been obtained in a divertor configuration both with deuterium gas flow and pumping, i.e. "puff and pump" [8] and with no deuterium flow or pumping during the impurity injection phase. To date, divertor discharges with argon impurity injection and D_2 puffing have achieved the highest densities.

High ℓ_i is an attractive scenario for the DIII-D advanced tokamak (AT) program because the stability limit in DIII-D is given by $\beta_N \approx 4\ell_i$ [9]. We have ob-

served a synergism between an increasing radiative fraction and ℓ_i i.e. a higher radiative fraction produces a more peaked current profile and higher ℓ_i. Thus radiating mantle discharges may make an attractive target plasma for high performance AT discharges. We note that ELMing H-mode discharges with $\beta_N H$ up to 8 for durations of more than 600 ms have been achieved with neon impurity puffing [10]. While core radiation and density in these discharges is higher than comparable discharges without neon or argon impurity radiation, the impurity fraction is still low, $P_{rad\_tot}/P_{in} < 0.5$, and a detailed discussion of these types of discharges is beyond the scope of this paper.

In summary, radiating mantle discharges have been obtained in DIII-D in both limiter and divertor configurations and in both L-mode and ELMing H-mode. However, operation at densities near the Greenwald limit for DIII-D limiter discharges has not been achieved, so the TEXTOR RI-mode confinement scaling ($\tau_E \propto n_e$) cannot be examined in DIII-D at the present time. Diverted radiating discharges in DIII-D have transiently achieved densities near the Greenwald limit with ELMing H-mode confinement and significantly reduced heat flux to the divertor region. The physical mechanisms contributing to this behavior have not been identified, but the roles of plasma rotation and suppression of electron gradient temperature modes [11] are under investigation. The radiating mantle discharges in DIII-D show that such scenarios may be desirable for future ignition machines.

Acknowledgements

Work supported by US Department of Energy under Contracts DE-AC03-89ER51114, DE-AC05-96OR22464, W-7405-ENG-48, and Grant DE-FG03-95ER54294. This work was also done as part of the DIII-D – TEXTOR collaboration supported by DOE and Euratom.

References

[1] E.A. Lazarus, J.D. Bell, C.E. Bush et al., Nucl. Fusion 25 (1985) 135.
[2] A.M. Messiaen, J. Ongena, B. Unterberg et al., Phys. Plasmas 4 (1997) 1690.
[3] O. Gruber, A. Kallenbach, M. Kaufmann et al., Phys. Rev. Lett. 74 (1995) 4217.
[4] M. Mori et al., Nucl. Fusion 28 (1988) 1892.
[5] B. Unterberg, A. Messiaen, J. Ongena et al., these Proceedings.
[6] B. Unterberg et al., Phys. Plasma (1998) EPS invited.
[7] G.L. Jackson, J. Winter, T.S. Taylor, Phys. Rev. Lett. 67 (1991) 3098.
[8] M.R. Wade et al., these Proceedings.
[9] E.J. Strait, Phys. Plasmas 1 (1994) 1415.
[10] G.L. Jackson, G.M. Staebler, D.R. Baker et al., Impurity Seeding and Radiating Mantle Discharges in the DIII-D Tokamak, to be presented at the 1998 APS-DPP meeting, November 1998.
[11] G.M. Staebler, G.L. Jackson, W.P. West et al., Energy Confinement Improved with Neon Injection in the DIII-D Tokamak, submitted to Phys. Rev. Lett. (1998).